Vapor Phase Metal-Assisted Chemical Etching of Silicon

Owen J. Hildreth and Daniel R. Schmidt*

This work introduces and explores vapor phase metal-assisted chemical etching (VP-MaCE) of silicon as a method to bypass some of the challenges found in traditional liquid phase metal-assisted chemical etching (LP-MaCE). Average etch rates for Ag, Au, and Pd/Au catalysts are established at 31, 70, and 96 nm/min respectively, and the relationship between etch rate and substrate temperature is examined experimentally. Just as with LP-MaCE, 3D catalyst motion is maintained and three-dimensional structures are fabricated with nanoparticle- and lithography-patterned catalysts. VP-MaCE produces less microporous silicon compared with LP-MaCE and the diffusion/reduction distance of Ag^+ ions is significantly reduced. This process sacrifices etch rate for increased etch uniformity and lower stiction for applications in micro-electromechanical systems (MEMS) processing.

1. Introduction

The ability to affordably fabricate arbitrarily complex three-dimensional geometries on the nanoscale is critical to the development and commercialization of numerous emerging technologies.[1,2] For example, technologies such as chiral photonics for advanced communication,[3] and nanofluidics for lab-on-a-chip applications[4,5] benefit from the fabrication and integration of 3D nanostructures. Unfortunately, nanofabrication techniques that scale economically for commercial applications are typically limited to fabricating either 1D or 2D structures with a high degree of geometric control, or 3D structures will little geometric control. These limitations restrict the impact that nanotechnology can have, and methods capable of fabricating large arrays of 3D structures in an affordable, scalable manner are needed.

Metal-assisted chemical etching (MaCE) of silicon has recently emerged as a new technique capable of fabricating arrays of reasonably complex 3D geometries in a single lithography/etch cycle.[6–11] Example structures include chiral 3D spiraling structures, spiraling nanopillars, vertically aligned thin-film metallic nanostructures, sub-surface curved nanohorns, and zig-zag nanowires.[6–13] The ability of MaCE to fabricate 3D structures results from a unique etching paradigm in which the object that defines the etch profile travels with the etch front, enabling extremely tight feature resolution over the entire etch length, taper angles less than 0.02°,[11] and the facile fabrication of 3D nanostructures. MaCE begins when a catalyst, such as Ag, Au, Pt, or Pd, is deposited or patterned on the silicon substrate and then immersed in a solution containing hydrofluoric acid (HF) and an oxidizing agent such as hydrogen peroxide (H_2O_2). On its own, this solution will not etch undamaged silicon at an appreciable rate; however, the metal serves as a catalyst for H_2O_2 reduction, a reaction that consumes two electrons and injects two holes (h^+) deep into the valance band of the silicon.[14] This creates a hole (h^+) rich region of silicon surrounding the metal catalyst that is readily oxidized by HF to form soluble SiF_6^{2-} and H_2SiF_6 with the reaction continuing as the catalyst is pulled into the substrate *via* van der Waals and electrostatic forces.[7,12,15,16] In short, the catalyst serves to generate a localized, traveling galvanic etching reaction, where 3D nanostructures are readily fabricated by designing catalysts that travel along predictable 3D paths.[6–9,11] A recent review article summarizes the effect of catalyst material, etchant composition, dopant levels, crystallographic orientation, and more.[17]

Any nanofabrication technique suitable for commercial manufacturing must exhibit a high degree of within-wafer uniformity and wafer-to-wafer reproducibility. We encountered processing challenges during our previous work fabricating chiral and out-of-plane structures using MaCE[7,8] that could lower the uniformity and reproducibility of MaCE processes. First, MaCE generates H_2 gas bubbles under many catalyst/etchant combinations. These bubbles create local differences in etch rate and non-uniformities in etch depth across the wafer. Solvents such as methanol can be used to lower the surface tension of the etchant and reduce the size of the H_2 bubbles;[9] however, the use of solvents does not completely eliminate the impact of H_2 gas generation nor are they compatible with the polymer pinning structures used in out-of-plane MaCE.[7,10] Fluid flow is the second processing challenge found in MaCE, as fluid flowing over the catalyst can influence the etching path of the catalyst. In our previous work, we were often limited to using small, 1 cm × 1 cm substrates to ensure that the MaCE etchant dropped onto the surface would be pinned by the edges of the substrate and any fluid flow would be minimized; however, this is not a viable option for wafer-scale fabrication.

This paper introduces and examines vapor phase MaCE (VP-MaCE) as an etching technique that bypasses the processing challenges detailed above. Inspired by Vapor Phase HF etching of SiO_2 substrates for micro-electromechanical systems

O. J. Hildreth
Electromagnetics Division
National Institute of Standards and Technology
Boulder, CO 80305, USA
E-mail: owen.hildreth@nist.gov
D. R. Schmidt
Quantum Electronics and Photonics Division
National Institute of Standards and Technology
Boulder, CO 80305, USA

DOI: 10.1002/adfm.201304129

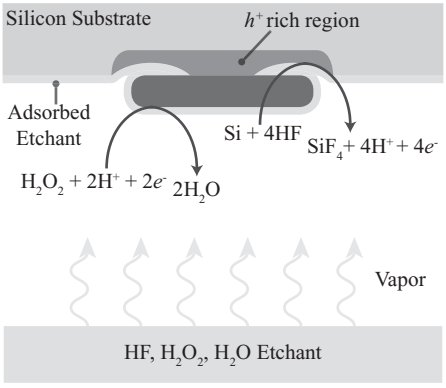

Figure 1. Schematic of VP-MaCE process. HF, H_2O_2, and H_2O vapor is adsorbed on the silicon and catalyst surface. H_2O_2 is reduced on the catalyst, creating a hole (h^+) rich region of silicon (Si^*) surrounding the metal catalyst. Si^* is oxidized by the adsorbed HF to form SiF_4. H_2O and SiF_4 vapor desorbs from the surface. Catalyst travels into the substrate regardless of wafer orientation.

(MEMS),[18–20] VP-MaCE delivers the etchant to the substrate surface in the vapor phase instead of the liquid phase. As schematically illustrated in **Figure 1**, HF, H_2O_2, and H_2O vapor from an etchant solution is adsorbed on the sample surface in a condensed thin layer less than 2 nm thick.[21,22] The proposed etching mechanism is similar to the LP-MaCE reaction proposed by Li et al.[14] with the substitution of $SiF_{4(gas)}$ as the end product instead of H_2SiF_6: Cathode reaction (at metal):

$$H_2O_2 \downarrow +2H^+_{(ad)} \rightarrow 2H_2O \uparrow +2h^+$$

Anode reaction (at silicon):

$$Si^{0+} + 4h^+ \rightarrow Si^{4+}$$

$$Si^{4+} + 4HF \downarrow \rightarrow SiF_4 \uparrow +4H^+_{(ad)}$$

Overall reaction:

$$Si^{0+} + 4h^+ \rightarrow Si^{4+}$$

This process provides a number of benefits over LP-MaCE. First, since the reactions proceed in a thin condensed layer, any gaseous byproducts readily diffuse out of the adsorbed layer and away from the substrate, eliminating any issues associated with bubble formation. Second, catalyst motion will be determined solely by near-surface forces, so inconsistencies due to fluid flow over the substrate surface are thus circumvented. Third, since VP-MaCE is a "dry" process, it can be used for stiction sensitive applications without the need for supercritical drying steps. An investigation of a small region of the parameter space was undertaken in order to evaluate this process. From this study, the etch rate of Ag, Au, and Pd/Au catalysts at one etchant composition are evaluated. This study also notes that, unlike many LP-MaCE systems, VP-MaCE does not form a layer of meso/microporous silicon preceding the metal catalyst. Lastly, this study establishes that catalysts in VP-MaCE still travel through 3D space and helical structures are readily fabricated with this process.

2. Results and Discussion

Ag, Pt, and Pd/Au (40/60 atomic percent) catalysts were deposited using electron beam deposition with a target thickness of 2.3 nm to 3.0 nm on separate p-type (5 – 10 Ω-cm), 100-mm diameter (100) silicon wafers. Samples scribed from the wafers and cleaned with either O_2 plasma or a piranha solution of 3:1 sulfuric acid:H_2O_2 immediately prior to etching to remove any adsorbed hydrocarbons and then etched with the vapor coming from a $\rho = 70^{12.8}$ etchant solution (≈ 27 °C). Note that ρ^x is used to denote the etchant composition where $\rho^x = ([HF]/([HF] + [H_2O_2]))^{x = [HF]}$ and x is the HF concentration in units of moles/liter. The samples were held approximately 25 mm above the etchant by use of an HF-compatible static chuck with substrate temperature control. The etch rate as a function of time was evaluated for 15, 30, 45, and 60 minutes with the substrate held at 40 °C. The influence of temperature was evaluated for Au catalysts etched for 15 minutes. The formation of microporous silicon in VP-MaCE versus LP-MaCE was examined by comparing samples etched with VP-MaCE at 35 °C held in the static chuck with samples held at room temperature above the solution to such that droplets form on the sample surface. Ag catalyst dissolution and re-deposition was confirmed by suing electron-beam lithography to pattern Ag and Au catalysts that were approximately 65 nm thick.

Silicon coated with metal catalysts and exposed to a vapor mixture of HF and H_2O_2 etch in a manner almost identical to LP-MaCE. Just as with LP-MaCE, etching is confined to a narrow, 1–2 nm region surrounding the catalyst with the etching process propagated by catalyst motion through 3D space. The main differences observed were a significant reduction in the etch rate and the lack of any observed microporous and mesoporous silicon etch front.[23,24] The scanning electron microscope (SEM) micrographs in **Figure 2** show VP-MaCE of Si etched with Ag, Au, and Pd/Au (columns) catalysts etched for 15, 30, 45, and 60 min (rows). The mean and maximum observed etch depths are provided in the upper left corner of each image, a dashed yellow line on some of the images indicates the location of the original surface for samples with significant surface etching. The nanoparticle catalysts were found to randomly etch through 3D space with a full six degrees of freedom, as seen with traditional LP-MaCE.[11] As a result, catalyst particles were observed over a wide range of depths even within a single sample with only a small percentage of the particles etched perpendicular to the catalyst surface over the entire etch and a significant number of catalysts remaining within the top 1– 2 μm of the surface. The plots in **Figure 3**a show the mean observed etch depth as a function of time for the three catalysts along with the linear fit used to estimate the average etch rate. The box plots in Figure 3b–d show the distribution of where catalyst particles were observed along with the fits from Figure 3a. The wide distribution in observed etch depth is attributed to the catalyst particles etching through 3D space along random directions.[11] The etch depth and rate data are summarized in **Table 1**. Importantly, no etching was observed in areas not covered by the catalyst.

From these results it is clear that the metal catalyst propagates the etching reaction and, while there is some dependence on catalyst material, this is not as pronounced as with

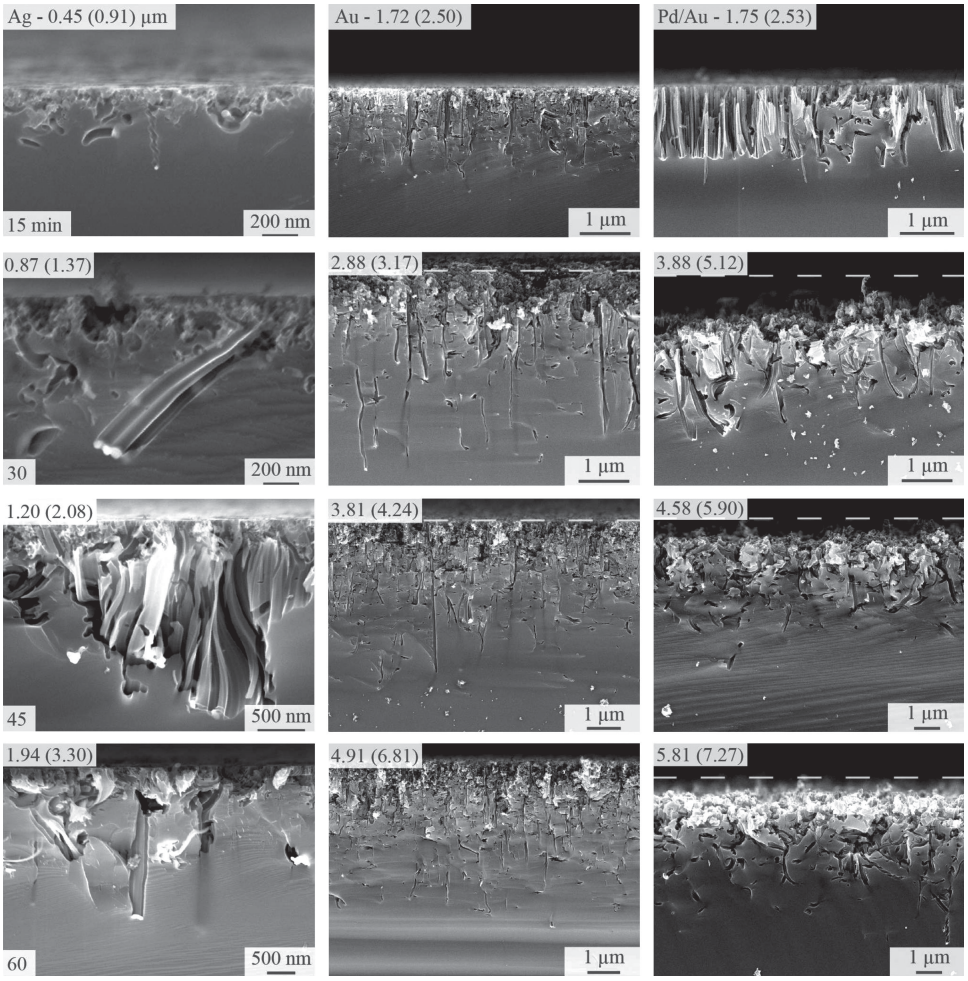

Figure 2. SEM micrographs of VP-MaCE etched silicon with Ag, Au, and Pd/Au catalysts (columns) for 15, 30, 45, and 60 min (rows). The mean and (max) etch depth are given in the upper left of each micrograph. A dashed yellow line indicates where the top of the sample was for those samples with considerable surface damage (reference point may be outside the image). All scale markers are 1 µm unless otherwise noted.

LP-MaCE. For example, Ag, Au, and Pd catalysts etch at 0.3, 5.0, and >30 µm/min in a $\rho = 90^{13.8}$ liquid phase etchant solution (4:1.3:2.7 HF:H_2O_2:H_2O),[23] scaling with the catalytic activity of the metal. However, the etch rates of Ag, Au, and Pd/Au in VP-MaCE drop to 0.03, 0.07, and 0.10 µm/min and do not show the order-of-magnitude scaling seen in LP-MaCE. This implies that the etching reaction is limited more by the concentration of HF and H_2O_2 within the condensed layer than the catalytic activity of the metal. For the $\rho = 70^{12.8}$ etchant solution used as an HF and H_2O_2 vapor source, the relative fractions of HF/H_2O_2/H_2O are 0.033/0.004/0.963. From literature, the partial pressure HF, H_2O_2, and H_2O of this mixture at 300 K can be estimated at 105 Pa, 13 Pa, and 3070 Pa respectively.[19,25,26] This gives an incoming etchant vapor a mixture of $\rho = 90^{0.04}$, which is 345× more dilute than the etchant concentrations we typically use in LP-MaCE.[7,8,11] As a result, the etch rate of VP-MaCE for metals such as Au, Pt, and Pd is set by the HF and H_2O_2 flux rather than their catalytic activity while the etch rate of metals such as Ag or Cu would still be limited by their lower catalytic activity. Future work will look at varying the HF and H_2O_2 partial pressures independently by bubbling N_2 gas through separate supplies of HF and H_2O_2 to better examine the kinetics of this process.

The etch rate of VP-MaCE depends on substrate temperature. The etch depth and rate data for Au catalyst samples etched for 15 minutes at substrate temperatures from 35 °C to 60 °C above a $\rho = 70^{12.8}$ solution are shown in **Figure 4**. The shape of this graph is similar to the "volcano plot" seen in

Table 1. Mean and Max etch depth and etch rates for Ag, Au and Pd/Au catalysts. Etch rates were calculated using a linear fit of mean and max etch depth vs. time for each catalyst. Since the catalyst can etch through 3D space, the mean and max values differ significantly as only a small portion of the catalysts will etch vertically along its entire etch path.

Catalyst	Mean/Max Etch Depth [µm]				Mean/Max Etch Rate [nm/min]
	15 min	30 min	45 min	60 min	
Ag	0.45/0.91	0.87/1.37	1.20/2.08	1.94/3.30	31/52
Au	1.72/2.50	2.88/3.17	3.81/4.24	4.91/6.81	70/110
Pd/Au	1.75/2.53	3.88/4.90	4.58/5.90	5.81/7.27	96/120

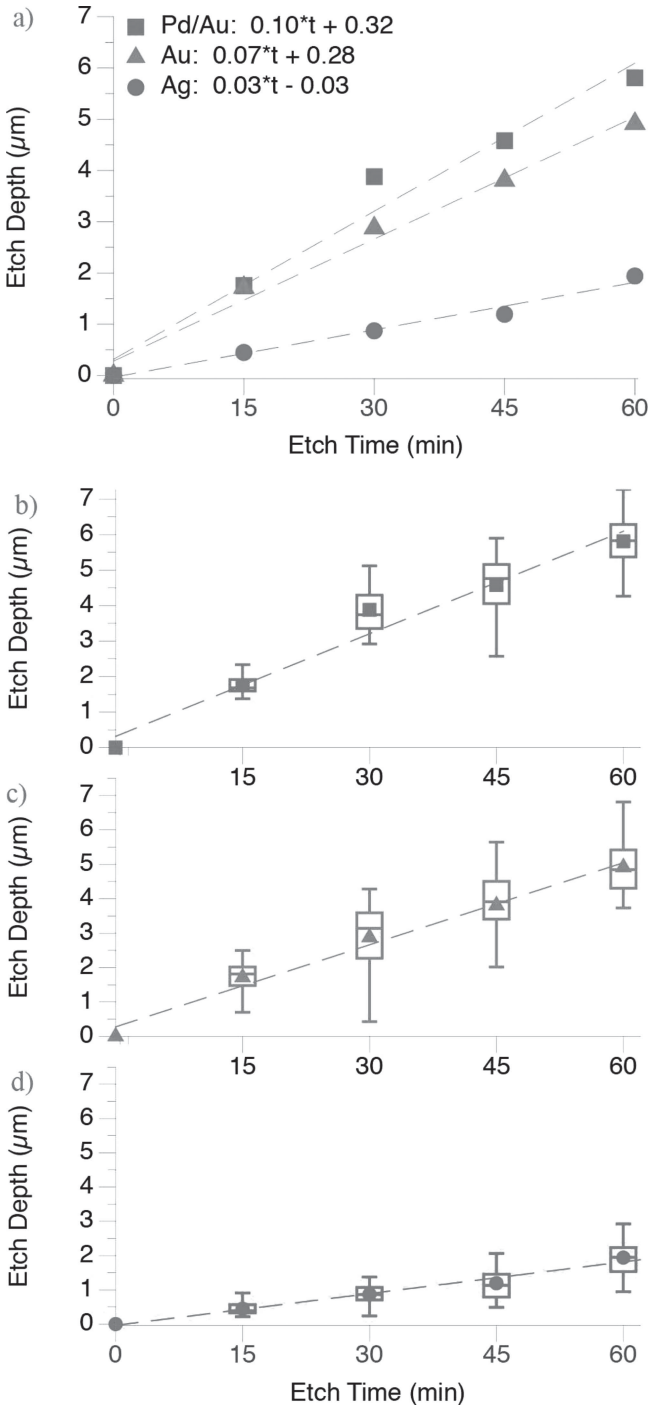

Figure 3. Graphs of etch depth versus time for Pd/Au (purple ■), Au (blue ▲), and Ag catalysts (red ●). (a) fitted mean etch depth. (b–d) box plots with fitted mean data for Pd/Au enabling extremely tight, Au, and Ag catalysts respectively. Notice that the etch rate of Ag is ~2–3 times smaller than that of Au and Pd/Au, while the etch rate of Au is only 20% smaller than that of Pd/Au. The large range in etch depth is due to the catalysts traveling through 3D space.

vapor phase HF etching of SiO_2,[20,26] although the maximum etch rate occurs at a slightly higher temperature of 40 °C instead of 35 °C.

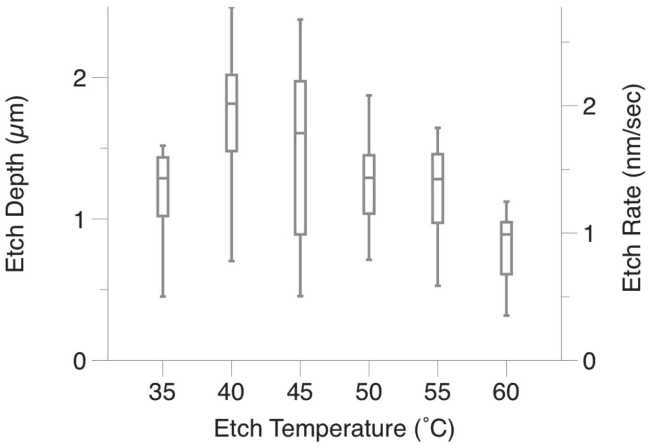

Figure 4. Box plots of etch depth and etch rate of Au catalysts versus substrate temperature after a 15-minute etch. VP-MaCE etch depth/rate dependence on substrate temperature is similar in shape to vapor phase HF etching of SiO_2. Notice that etch depth and rate follow a similar "volcano" shaped dependence on temperature similar to that of vapor phase HF etching of SiO_2.[18,26]

2.1. Catalyst Motion

As with LP-MaCE, catalysts travel through 3D space during the etching process, as exemplified by the helical structure shown in **Figure 5**. This observation leads to a number of important implications. First, 3D structures should be just as simple to fabricate with VP-MaCE as with LP-MaCE, ensuring that VP-MaCE could be used to fabricate complex structures without the stiction issues seen in liquid phase etching. Second, these results imply that the mechanisms driving catalyst motion in VP-MaCE are similar to LP-MaCE with catalyst motion driven largely by the near-surface interactions encompassed by the Derjaguin and Landau, Verwey and Overbeek (DLVO) model.[7] However, the thin, 1–2 nm thick condensed layer may result in

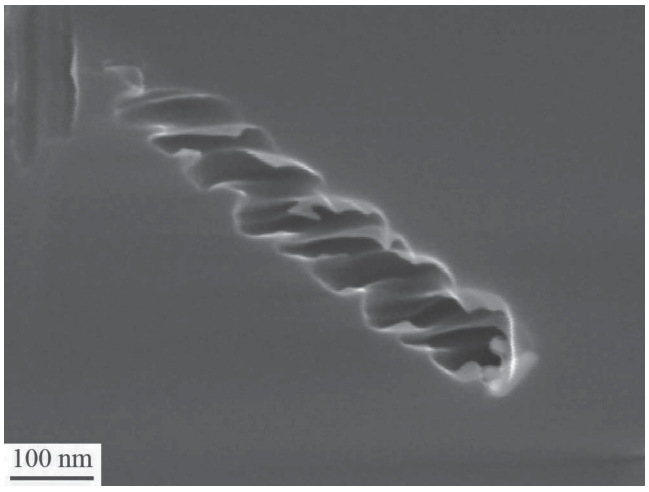

Figure 5. SEM micrograph of helical structure formed by a spiraling catalyst illustrating that catalysts still travel through 3D space during VP-MaCE. Notice that the etched channel closely follows the shape of the catalyst and that VP-MaCE maintains the extremely tight feature resolution of traditional LP-MaCE.

additional capillary forces at the liquid-solid-vapor interface and more study is needed to understand the impact these forces will have on catalyst motion in LP-MaCE. Third, the dynamic nature of catalyst motion will need to be accounted for when trying to etch specific structures. For example, to etch solely in the vertical dimension, one may need to adjust the HF and H_2O_2 concentrations within the incoming vapor and possibly adjust the catalyst shape and particle-to-particle spacing. Figure 5 also shows that the feature resolution of VP-MaCE is at least equal to that of traditional LP-MaCE and the shape of the channel closely matches the shape of the catalyst particle.

2.2. Microporous Silicon

The formation of micro- and mesoporous silicon during LP-MaCE is a well-documented phenomena that occurs over a wide range of etchant, catalyst, and substrate combinations.[14] This porous silicon is the result of relatively complex interactions between competing Si oxidation routes (divalent, tetravalent, or oxidation to SiO_2 first by H_2O),[16,27] changes in band structure limiting hole (h^+) transport into nanostructured silicon,[27] localized band bending at the Si/metal interface,[28] and small differences in these processes as a function of crystallographic orientation.[29,30] While some applications, such as light absorption and photoluminescence, benefit from the formation of microporous silicon, it is usually unwanted for applications that require single-crystal silicon such as Si nanowire formation and MEMS.

VP-MaCE does not generate micro/mesoporous silicon at the etchant composition and delivery conditions used in this study: opening up MaCE processing to applications that require high-quality silicon. The micrographs in **Figure 6** illustrate the difference in microporous silicon generated in LP-MaCE versus VP-MaCE. Both of these samples consisted of 2.3 nm of Pd/Au deposited at the same time in an e-beam evaporator, then etched above the same $\rho = 70^{12.8}$ mixture. LP-MaCE was conducted by leaving the substrate at room temperature (~27 °C) to create a condensed layer on the substrate that is thick enough to slightly bead up on the surface. This thickly condensed layer had a similar etchant composition and concentration as compared to the VP-MaCE, yet results in a radically different morphology. The light grey areas surrounding the metal catalyst in Figure 6a are indicative of micro/mesoporous silicon generation, establishing that the LP-MaCE with a Pd/Au catalyst generates micro/mesoporous silicon even for extremely dilute etchant compositions. However, increasing the substrate temperature slightly reduces the condensed phase thickness to 1–2 nm, while maintaining the same etchant composition. As shown in Figure 6b, these samples show no any sign of micro/mesoporous silicon. These results have two important implications. First, VP-MaCE does less damage to the silicon surrounding the metal catalyst and may be more suitable than LP-MaCE for applications that require high-quality, undamaged silicon. Second, the electrical double layer at the etchant/Si interface may play a larger role in the formation of micro/mesoporous silicon than previously thought and, while there are numerous references to hole (h^+) transport and confinement within the silicon leading to micro/mesoporous silicon generation,[16,28,31,32] we could not find any studies discussing the role that the electrochemical double layer has on the formation of micro/mesoporous silicon. These phenomena are still under investigation and will be discussed in a future article.

2.3. Ag Catalyst Dissolution and Redeposition

The dissolution and re-deposition of silver catalysts in LP-MaCE reduces feature resolution.[16,24] This study confirms that the same issue exists for VP-MaCE and that Ag ions form within the thin condensed layer of etchant and travel far enough to dramatically change the shape of the deposited catalysts. This is exemplified by the micrographs in **Figure 7** showing the shape of catalysts patterned using electron beam lithography (EBL) before etching (Figure 7a) along with post-etch

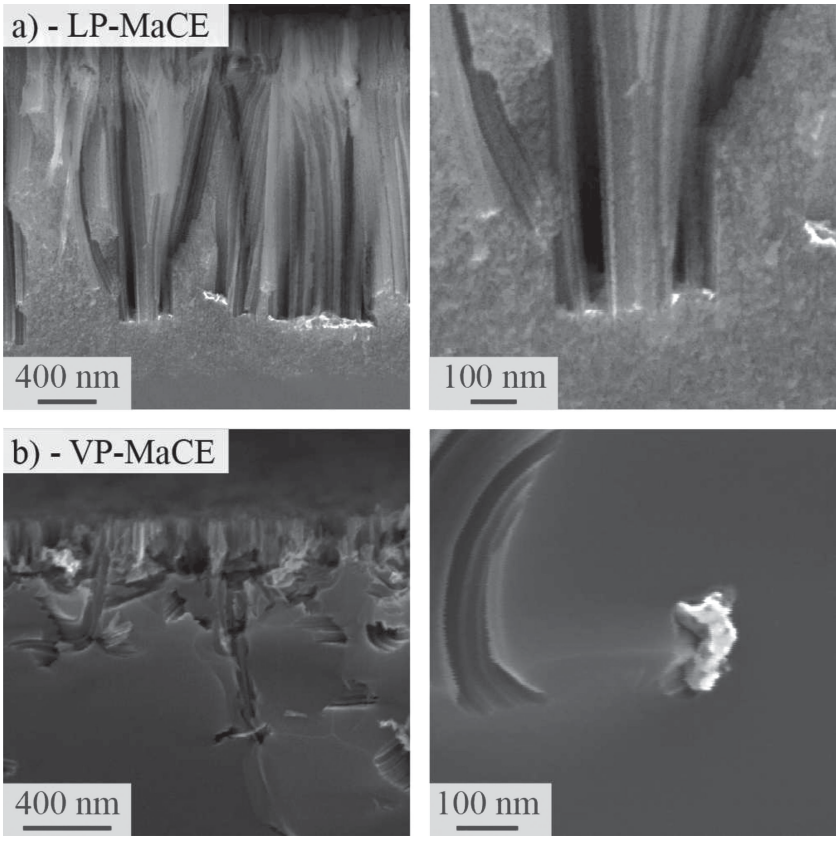

Figure 6. SEM micrographs of Si etched with Pd/Au catalysts when (a) LP-MaCE and (b) VP-MaCE is used with both substrates held at similar etchant compositions within the condensed layer. The light grey/white areas surrounding the metal catalysts (bright white) indicate the formation of microporous silicon. These light-grey areas are missing in the VP-MaCE samples, indicating that VP-MaCE does not generate microporous silicon.

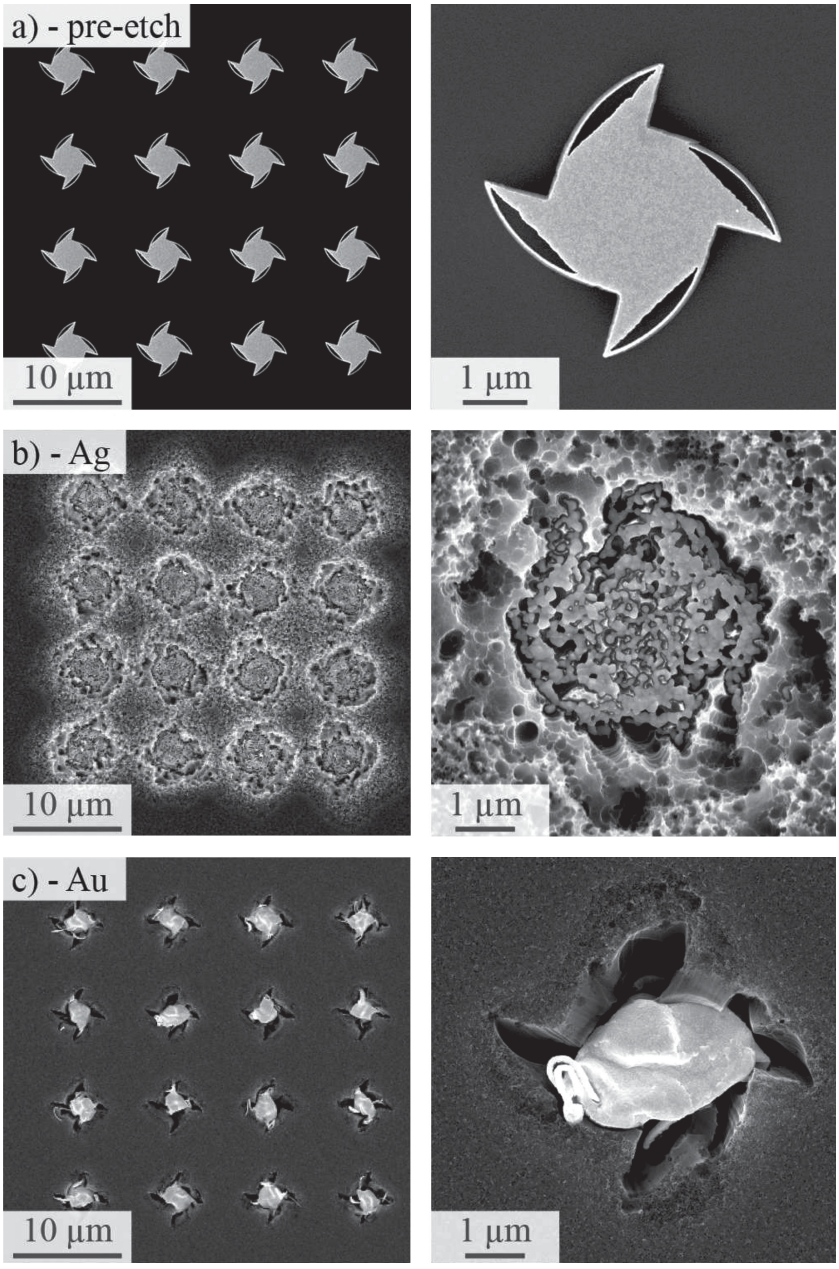

Figure 7. SEM micrographs illustrating the difference in catalyst stability between Ag and Au catalysts. (a) Original, pre-etch structure. (b) Ag catalysts form small Ag particles and clusters as Ag is dissolved and re-deposited during VP-MaCE. (c) Au catalysts remain whole although deformed, because the catalyst was too thin to withstand the large DLVO and capillary forces involved in VP-MaCE.[7]

micrographs of Ag and Au catalysts (Figure 7b,c). The Ag catalyst clearly decomposes into small pieces with some pieces etching independent paths through the surrounding catalyst, while the Au catalyst remains whole and, as expected for a 60 nm thick catalyst,[7,8] deforms into a small ball under the influence of the large DLVO forces that drive catalyst motion. The results with the Ag catalyst are particularly noteworthy in that, combined with recent results by Geyer et al.,[24] we now have conclusive proof that Ag catalysts in MaCE are oxidized by HF to form Ag^+ ions that diffuse some distance before being reduced to $Ag_{(metal)}$ through Si oxidation by HF on the silicon surface.

3. Conclusion

Metal-assisted chemical etching works in the vapor phase. Feature resolution was comparable to liquid phase MaCE and on the order of 1–2 nm for stable catalysts. The low etchant concentration results in a significantly lower etch rate compared with LP-MaCE conducted with high concentrations of HF and H_2O_2. The etch rate varied with substrate temperature, forming the familiar volcano shape seen in vapor phase HF etching of SiO_2. Critical to 3D nanofabrication, catalysts do travel through 3D space during VP-MaCE, and helical structures were routinely observed in this experiment. VP-MaCE does not form microporous silicon as is often seen with LP-MaCE, further increasing the resolution and utility of MaCE processes. Lastly, we demonstrated that Ag catalysts form Ag^+ ions that diffuse through the thin condensed layer and redeposit elsewhere on the silicon substrate.

This work expands the capabilities of MaCE and significantly reduces problems with stiction seen with LP-MaCE while also completely inhibiting the formation of micro/mesoporous silicon. This process should enable the fabrication of even higher aspect ratios and with stronger mechanical properties.

4. Experimental Section

All samples were prepared from p-type, 100-mm diameter (100) silicon wafers with a manufactured stated resistivity of 5–10 Ωcm. Ag, Au, and Pd/Au (40/60 atomic percent) were deposited on separate wafers using an electron beam evaporator for a target thickness of 2.3–3.0 nm at 0.15 nm/s and then 1 cm × 1 cm samples were scribed from the larger wafer. Immediately prior to etching, samples were cleaned with either O_2 plasma or a piranha mixture of 3:1 sulfuric acid:H_2O_2. This cleaning step is extremely important as VP-MaCE was found to be more sensitive than LP-MaCE to adsorbed hydrocarbons reducing the catalytic activity of the metal particles. Samples were etched with the vapor coming from a $\rho = 70^{12.8}$ etchant solution made with 16 mL of 48 wt% HF and 18.4 mL of 30 wt% H_2O_2. Note that ρ^x is used to denote the etchant composition where $\rho^x = ([HF]/([HF] + [H_2O_2]))^{x = [HF]}$ and x is the HF concentration in units of moles/liter. The etchant was held at room temperature (≈27 °C) and the samples were held approximately 25 mm above the etchant by use of an HF-compatible static chuck with substrate temperature control.

To evaluate the etch rate as a function of time, samples were etched at 40 °C for 15, 30, 45, and 60 min. To evaluate the influence of temperature, Au catalysts were etched for 15 min at 35, 40, 45, 50,

55, and 60 °C. The formation of microporous silicon in VP-MaCE versus LP-MaCE was examined by comparing samples etched with VP-MaCE at 35 °C held in the static chuck with samples held at room temperature above the solution. The sample held at room temperature forms a thicker condensed liquid layer that is visible to the eye. Ag catalyst dissolution and re-deposition was confirmed by using electron-beam lithography to pattern Ag and Au catalysts that were approximately 65 nm thick.

Top-down and cross-section images of the samples were taken using the In-Lens detector of a Ziess LEO 1525 Thermally-Assisted Scanning Electron Microscope (SEM) to determine etch depth, etch rate, hole morphology, and microporous silicon generation.

Acknowledgements

The manuscript was written through contributions of all authors. All authors have given approval to the final version of the manuscript.

Received: December 10, 2013
Revised: January 21, 2014
Published online: March 14, 2014

[1] T. G. Leong, A. M. Zarafshar, D. H. Gracias, *Small* **2010**, *6*, 792.
[2] S. M. Weiss, M. Haurylau, P. M. Fauchet, *Optical Mater.* **2005**, *27*, 740.
[3] M. Thiel, M. Decker, M. Deubel, M. Wegener, S. Linden, G. von Freymann, *Adv. Mater.* **2007**, *19*, 207.
[4] F. Romanato, M. Tormen, L. Businaro, L. Vaccari, T. Stomeo, A. Passaseo, E. Di Fabrizio, *Microelectron. Eng.* **2004**, *73*, 870.
[5] Y. Wang, W.-Y. Lin, K. Liu, R. J. Lin, M. Selke, H. C. Kolb, N. Zhang, X.-Z. Zhao, M. E. Phelps, C. K. F. Shen, K. F. Faull, H.-R. Tseng, *Lab on a Chip* **2009**, *9*, 2281.
[6] O. Hildreth, C. Honrao, V. Sundaram, C. P. Wong, *ECS Solid State Lett.* **2013**, *2*, P39.
[7] O. Hildreth, K. Rykaczewski, A. G. Fedorov, C. P. Wong, *Nanoscale* **2013**, *5*, 961.
[8] O. Hildreth, A. G. Fedorov, C.-P. Wong, *ACS Nano* **2012**, *6*, 10004.
[9] K. Rykaczewski, O. Hildreth, C. P. Wong, A. G. Fedorov, J. H. J. Scott, *Nano Lett.* **2011**, *11*, 2369.
[10] O. Hildreth, D. Brown, C. P. Wong, *Adv. Funct. Mater.* **2011**, *21*, 3119.
[11] O. Hildreth, W. Lin, C.-P. Wong, *ACS Nano* **2009**, *3*, 4033.
[12] K. Tsujino, M. Matsumura, *Electrochem. Solid St.* **2005**, *8*, C193.
[13] H. Chen, H. Wang, X.-H. Zhang, C.-S. Lee, S.-T. Lee, *Nano Lett.* **2010**, *10*, 864.
[14] X. Li, P. W. Bohn, *Appl. Phys. Lett.* **2000**, *77*, 2572.
[15] B. Cappella, P. Baschieri, C. Frediani, P. Miccoli, C. Ascoli, *Engineering in Medicine and Biology Magazine* **1997**, *16*, 58.
[16] C. Chartier, S. Bastide, C. Levy-Clement, *Electrochim Acta* **2008**, *53*, 5509.
[17] Z. Huang, N. Geyer, P. Werner, J. de Boor, U. Gösele, *Adv. Mater.* **2011**, *23*, 285.
[18] P. Munter, O. Aepli, R. Kossatz, *Ind. Eng. Chem.* **1947**, 39, 427.
[19] P. A. Munter, O. T. Aepli, R. A. Kossarz, *Ind. Eng. Chem.* **1949**, *41*, 1504.
[20] Y. Fukuta, H. Fujita, H. Toshiyoshi, *Microelectronics and Reliability* **2003**, *42*, 3690.
[21] B. H. Claussen, *J. Electrochem. Soc.* **1964**, *111*, 646.
[22] D. B. Asay, S. H. Kim, *J. Phys. Chem. B* **2005**, *109*, 16760.
[23] O. Hildreth, Development of Metal-assisted Chemical Etching of Silicon as a 3D Nanofabrication Platform, Georgia Institute of Technology, Atlanta **2012**, pp. 1–279.
[24] N. Geyer, B. Fuhrmann, H. S. Leipner, P. Werner, *ACS Appl. Mater. Interfaces* **2013**, *5*, 4302.
[25] S. L. Manatt, M. R. R. Manatt, *Chem.—Eur. J.* **2004**, *10*, 6540.
[26] C. R. Helms, *J. Vac. Sci. Technol. A* **1992**, *10*, 806.
[27] R. L. Smith, S. Collins, *J. Appl. Phys.* **1992**, *71*, R1.
[28] Z. Huang, N. Geyer, L. F. Liu, M. Y. Li, P. Zhong, *Nanotechnology* **2010**, *21*, 465301.
[29] K. Peng, A. Lu, R. Zhang, S.-T. Lee, *Adv. Funct. Mater.* **2008**, *18*, 3026.
[30] Z. Huang, T. Shimizu, S. Senz, Z. Zhang, N. Geyer, U. Goesele, *J. Phys. Chem. C* **2010**, *114*, 10683.
[31] D. Gruen, T. Knickerbocker, T. Lasseter, J. Russell, *Adv. Mater.* **2004**, *17*, 1045.
[32] K. Peng, H. Fang, J. Hu, Y. Wu, J. Zhu, Y. Yan, S. T. Lee, *Chem.—Eur. J.* **2006**, *12*, 7942.